Chemical Engineering Science 131 (2015) 187–196

Contents lists available at ScienceDirect

Chemical Engineering Science

journal homepage: www.elsevier.com/locate/ces

# Can acoustic emissions be used to size bubbles seeping from a sediment bed?

A. Vazquez [a,*], R. Manasseh [b,c,d], R. Chicharro [a]

[a] Universidad Nacional Autónoma de México – Facultad de Ciencias, Laboratorio de Fluidos, Av. Universidad 3000, Delegación Coyoacán, C.P. 04510 México, D.F., Mexico
[b] Department of Mechanical and Product Design Engineering, Faculty of Engineering & Industrial Sciences, Swinburne University of Technology, Hawthorn, Melbourne, Vic. 3122, Australia
[c] Department of Mechanical Engineering, University of Melbourne, Melbourne, Vic. 3010, Australia
[d] Fluid Dynamics Group, CSIRO Materials Science and Engineering, PO Box 56, Highett, Melbourne, Vic. 3190, Australia

## HIGHLIGHTS

- We generated air bubbles in a sediment bed in the laboratory.
- Gas interactions are recorded simultaneously by hydrophone and high speed camera.
- The acoustical signals are analyzed by power spectra and sonogram methodologies.
- Sediment interaction, elastic resistance and asymmetric gas detachment are showed.
- Underwater acoustic sensors could warn of critical changes in bubble-seep behavior.

## ARTICLE INFO

*Article history:*
Received 28 October 2014
Received in revised form
13 March 2015
Accepted 22 March 2015
Available online 11 April 2015

*Keywords:*
Acoustic signals
Bubble detachment
Gas seeps
Hydrophone
Power spectra
Sediment bed

## ABSTRACT

Experiments on bubble formation from a granular medium are presented. The granular medium consisted of immersed stones giving a sediment bed thickness of 10 cm. High speed photographic and acoustic passive wireless techniques were employed to obtain the bubble size. The power spectra of the acoustic data for bubble production of 0.5 bubbles/s showed the existence of two principal peaks which are correlated with two discrete events. Firstly, a signal peak at 0.497 kHz, representing asymmetric bubble detachment, and secondly, a peak at 2.070 kHz, which corresponded to interactions of the granular media as inter-particle gaps advance, representing elastic resistance to orifice creation. Provided the signals were windowed to the bubble-detachment event only, the classical bubble-acoustical Minnaert relation for the bubble size agreed with optical data within about 10%. Since seepage generates discrete bubble pulses, appropriate acoustic analyses could both count and size the bubbles formed. The results of this study lead to the proposition that underwater acoustic sensors could warn of critical changes in bubble-seep behavior over time. This could lead to the possibility of remote early warnings, because shifts in production-rate regimes from seeps may herald alterations in the progression of global warming, or impending earthquakes and tsunamis.



## 1. Introduction

Recently it has been found that methane trapped in permafrost is escaping the sea bed from wide areas of the East Siberian shelf (Shakhova et al., 2005) and is an important accelerator of global warming (MacGuire et al., 2006). Methane may migrate through the sediment as either a dissolved or a free gas phase, creating bubble plumes, and gases emitted from the decay of organic matter in marine sediments also may contribute to global greenhouse gas budgets (Arndt et al., 2013). The methane bubbles are generated in geological structures called marine seeps or pockmarks which contribute 0.4–48 tera grammes per year of methane to the hydrosphere and atmosphere (Judd and Hovland, 2007). The marine seeps are located on the seabed and generally percolate through sediments (siliceous, calcareous, pelagic clay, land-formed, etc.). The ability to monitor such seeps over long periods of time would give information about local gas fluxes and their temporal and spatial variation (Judd, 2004).

Furthermore, it has been recognized for some time that monitoring of the emission of gases near faults may assist earthquake

* Corresponding author. Tel.: +52 55 5622 4934.
*E-mail address:* zeta24_75@yahoo.com (A. Vazquez).

http://dx.doi.org/10.1016/j.ces.2015.03.058
0009-2509/

prediction (Sugisaki, 1981; Hartmann and Levy, 2005). Changes in undersea gas seepage may be earthquake precursors (Khilyuk and Chilingar, 2000). Emissions of radon vapor and its decay products from the Earth's crust, in wells and spring water along active fault zones, have been recognized as a potential tool in earthquake prediction (Klusman and Webster, 1981; Papastefanou, 2007). Thus, underwater bubble formation in terrestrial springs and lakes should also benefit from monitoring.

Zones of the ocean bottom which generally show microseismic activity can be monitored by an array of geophones (Webb et al., 2001). This technology, commonly used to studying the structure of the upper mantle, is now applied to the oceanic crust using natural earthquakes as sources. The Ocean-Bottom Seismometers (OBS) record high-fidelity seismic data for long periods of time. Gas seeps offer an additional source of data enhancing the predictive power of long-term monitoring. In the course of a dedicated research cruise, it is possible to locate gas seeps using active acoustical methods such as vessel-mounted sonar (Matveeva et al., 2003; Schneider von Deimling et al., 2007; Artemov et al., 2007; Nikolovska et al., 2008). However, active devices are expensive and inherently require significant power to operate and hence cannot be left for long periods of time on the seabed.

Some studies (Nikolovska and Waldmann, 2006; Leighton and White, 2012) have used the Passive Acoustical (*PA*) technique to obtain the bubble-size populations from undersea bubble plumes, with the objective of gas flux quantification. Generally, sparged bubbles are generated using rigid orifices (capillary tubes, perforated plates, ceramic stones, etc.) but in the granular case, the orifice behavior is affected by the air flow rate, particle diameter, particle density and the frictional forces (mobility) between particles (Gostiaux et al., 2002). When air is injected into a sediment bed, the gas penetration is resisted by capillary pressure as the gas invades the interstitial spaces. In addition, it is also known that if the bubbles are generated in microbial clay sized particles of ≈ 3.9–62.5 μm (a by-product of metabolism by methanogenic bacteria methane; see Floodgate and Judd, 1992), the particle size can affect the bubble dynamics, that is, if the bubbles are small relative to particle size, they remain within the pore fluid and behave as bubbles in water, on the other hand, if bubbles are large relative to particle size the structure of the sediment frame interacts with the bubbles and changes the bubble compressibility (Wilkens and Richardson, 1998). *PA* techniques are also applied in the laboratory (Vazquez et al., 2008) and in industries (Boyd and Varley, 2001; Manasseh and Ooi, 2009) in systems in which bubbles are generated by diverse devices: capillary tubes, ceramic stones, perforated plates, plastic membranes, metallic mesh, granular materials, sediments, etc. The bubble generation can have a great influence on the formation size and hence subsequent behavior when bubbles rise through the water (Leighton, 1994; Leighton et al., 1991).

The simplest class of data likely to be of practical relevance to long-term monitoring is the volumetric gas flow from a seabed source, *Q*, although the gas composition may also be relevant (Fu et al., 2005). The flow rate is equal to the volume of each bubble produced multiplied by the rate at which bubbles are produced; in situations where variable bubble sizes are generated, this can be expressed as

$$Q = \sum_{i}^{N} \frac{4}{3}\pi {R_{0i}}^3 f_{bi}, \tag{1}$$

where $R_{0i}$ is the equivalent-spherical radius of the $i$th bubble, $N$ is the number of bubbles and $f_{bi}$ is the rate at which the bubbles are formed. In order to reliably and accurately monitor gas seepage, accurate measures of both bubble size and the rate of bubble production are needed. To achieve this, the acoustic signals corresponding to the formation of individual bubbles generated at low gas flow rates must be separated from other confounding signals due to sediment motion or background noise (or other marine noises such as that due to the breaking wave, or bubbles bursting the sea surface, etc.). Low gas flow rates are studied to preclude errors due to overlapping bubble signals, i.e. to preclude bubble coalescence or jetting regimes (Manasseh et al., 2008; Leighton and White, 2012). Since bubble-acoustic signals from bubble formation points fall off rapidly with distance from the source (Manasseh et al., 2008) appropriate placement of hydrophones close to individual, low gas-flow seeps would provide the most accurate data and hence the greatest dynamic range. The bubbles could then be counted and sized.

The core of the present *PA* methodology is based on bubble detachment from an orifice or capillary tube, i.e., when the bubbles are growing attached to an orifice. The subsequent inflation leads to the appearance of a neck, which connects the bubble's body to the orifice (Czerski and Deane, 2011; Deane and Czerski, 2008; Deane and Stokes, 2008). When the buoyancy force exceeds the other applicable forces (surface tension, drag, and pressure) (Vazquez et al., 2010), the neck finally breaks and a pulse of sound propagates through the fluid (the origin of the sound has been explained in the literature by three separate mechanisms, summarized in Manasseh et al. (2008)); one mechanism possibly relevant to the present experiments is compression of gas in the bubble by a radial inrush of liquid as the pinch-off occurs (Deane and Czerski, 2008). The Minnaert relation (Minnaert, 1933) is used to relate the bubble size with the sound wave frequency,

$$f_0 = \frac{1}{R_0}\sqrt{\left(\frac{3\gamma P_A}{4\pi^2\rho}\right)} \tag{2}$$

where $f_0$ is the frequency in Hz, $P_A$ is the absolute liquid pressure, $\rho$ is the liquid density and $\gamma$ is the ratio of specific heats for the gas assuming adiabatic compression and expansion, which is valid for millimetric bubbles. It is interesting to note that $\gamma$ takes the ideal-gas values of 1.67 ($\frac{5}{3}$) for monatomic gases (e.g. Rn), 1.4 ($\frac{7}{5}$) for diatomic gases (e.g. $N_2$), 1.3 ($\frac{9}{7}$) for triatomic gases (e.g. $CO_2$) and 1.2 (13/11) for $CH_4$ (Langes Handbook (Lange, 1999)). Thus, changes in gas composition may also cause changes in $f_0$, e.g. obtain low values of the frequency if $CH_4$ concentration were to increase. The Minnaert relation assumes several aspects such as a spherical bubble shape, that the mass-inertial contribution is only due to the liquid (the liquid density is much greater than the gas density), that the surface tension forces are negligible, the liquid is incompressible and that the bubble is surrounded by pure liquid and not particles with their own dynamics. Nonetheless, the Minnaert frequency has been widely and successfully used by many researchers (Boyd and Varley, 2001; Al-Masry et al., 2005; Chicharro and Vazquez, 2014) to obtain bubble sizes in diverse situations. What happens if the bubble is surrounded by a complex micro-environment of mobile solid particles as well as liquid? The answer to this question remains unclear so far, and leads to the goal of the present paper: a preliminary assessment of the feasibility of precise, long-term quantitative monitoring of a sediment bed.

We realized a preliminary and simple experiment (detailed below) using a granular-sediment bed in a Plexiglass tank. Air was injected at a rate (0.1 $cm^3/s$) at which there was only a single bubble in the tank at a time (the solitary flow rate), and at low (0.5 $cm^3/s$), medium (2.5 $cm^3/s$) and high (4.5 $cm^3/s$) rates. Bubble-detachment images and sound were recorded simultaneously by a high speed camera and wireless hydrophone. Finally the passive acoustic signal obtained from bubble generated from sediment bed was compared to the equivalent signal for a rigid orifice.

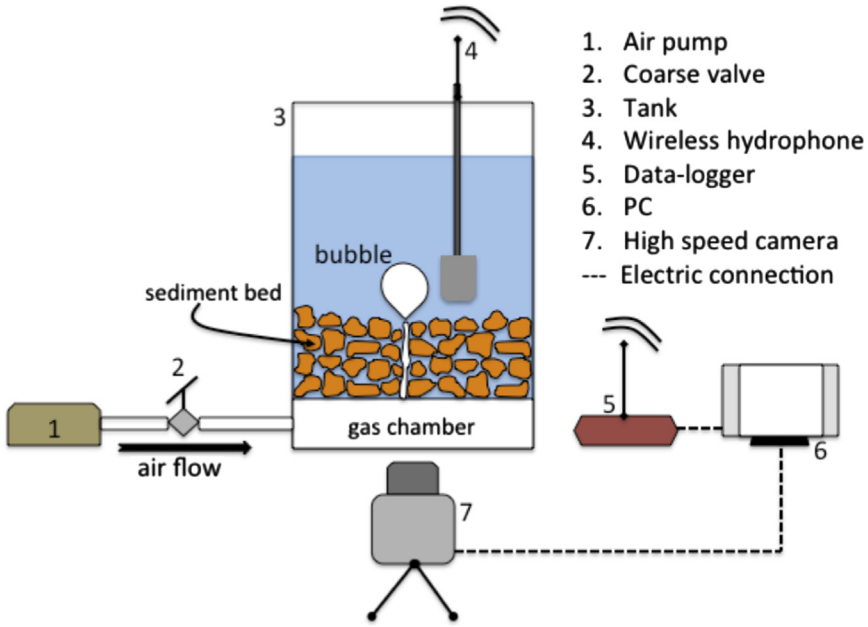


**Fig. 1.** Experimental apparatus.

## 2. Experimental apparatus and procedure

### 2.1. The equipment

The experimental setup (Fig. 1) consisted of a 5.3 W air pump (Atlantis Force, Mod. 12858, Taiwan) which sent an air flow to a gas chamber ($2\times10^{-3}$ m$^3$) controlled by a bronze coarse valve. Thus, the bubbles were air (i.e. $\gamma=1.4$). The acoustic signals generated during the bubble growth and departure from the sediment bed were measured with a custom built wireless piezoelectric hydrophone (Vazquez et al., 2005) and recorded by a data-logger (USB-6501, National Instruments, USA). The tank dimensions ($0.2\times0.2\times0.3$ m$^3$) were large enough to neglect acoustic coupling reverberation for millimeter-sized bubbles with walls (e.g. Manasseh et al., 2008). The working liquid was distilled water; salt water was not employed because it does not have great significance on the signature of the acoustic signal, though perhaps a minor effect on sound pressure (Kolaini, 1999). The water has a dynamic viscosity and density of 0.001 Pa s and 998 kg/m$^3$ respectively (taken from tables). As noted above, four bubble production rates were used, solitary (0.1 cm$^3$/s), low (0.5 cm$^3$/s), medium (2.5 cm$^3$/s) and high (4.5 cm$^3$/s) air flow rates. For solitary bubbles the rate of bubble production, $f_b$ was 0.5 bubbles s$^{-1}$. The hydrophone probe was located 5 cm away from the bubble, an optimum distance that minimized the perturbation to the bubble behavior (formation and detachment), while maximizing the signal to noise ratio (SNR) of the acoustic signal as much as possible. Finally the bubble images were obtained using a high speed color camera (Olympus i-SPEED, Olympus KeyMed, Ltd., United Kingdom) at 500 frames s$^{-1}$. These were synchronized with the acoustic signal-capture with all data stored by a notebook PC. The equivalent-spherical radius for the granular material was defined as $r_{eq}=(A/\pi)^{1/2}$, in which $A$ is the image area of each sediment particle and was calculated by ImageJ version 1.40f (National Institutes of Health, USA). It is important to mention that the area calculation was made considering the granular medium as a two-dimensional system, which is idealized since the sediment is actually a 3D-system and is known to exhibit contact forces between solids.

**Table 1**
Physical parameters of granular sediment.

| Tezontle | Spherical equivalent radius (mm) | Density bed (g/cm$^3$) | Circularity | Porosity ($\varphi$) |
|---|---|---|---|---|
| Igneous rock | $3.2\pm0.52$ | $1.56\pm0.09$ | $0.66\pm0.10$ | $0.28\pm0.11$ |

### 2.2. Granular media and orifice behavior

The granular bed (10 cm thickness) used was composed of tezontle (spherical-equivalent radius of 3.2 mm) which is a porous, extrusive, igneous and volcanic rock used extensively as construction material. The principal chemical composition of tezontle stones is an iron oxide, and they have a low density (owing to the porosity) and high lift behavior. Some important characteristics used for the tezontle particles in this study are summarized in Table 1. Clearly, not all material sediment particles will have the same properties as tezontle. The tezontle has a density of 1.2–1.6 g cm$^{-3}$. This may be compared to the sediment observed in field studies (e.g. Bridgwater Bay, North Somerset, UK, in Boudreau et al., 2005) which were clay and carbonate sands with a density of 1.3–1.7 and 2.7–2.9 g cm$^{-3}$ respectively. Thus the density of the material we use may be comparable to the density of some particles an oceanographic context. However, from the perspective of the present paper, the key material attribute is that the particle is rigid, since the proximity of a rigid surface is known to affect the acoustic behavior of nearby bubbles (Strasberg, 1953; Payne et al., 2011), and the key material property in addition to the density is the particle size, which would affect the particle motion.

When the gas force moves the tezontle particles the result is a fractured appearance in the bed, and subsequently the surface particles (located below the fracture) may be moved laterally and this particle mobility establishes an orifice (this is facilitated by the low density of the tezontle particles). In this sense, the orifice behaves as a half-door when the bubble is growing, so we call it a gate-orifice.

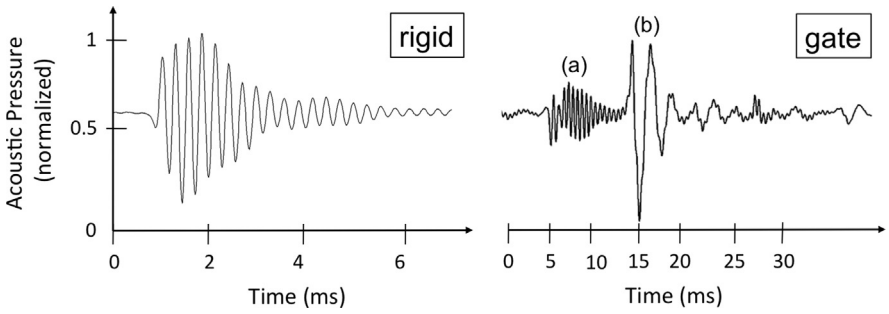


**Fig. 2.** Acoustic responses for bubble detachment from a classical rigid orifice and sediment bed respectively.

## 3. Results

### 3.1. Acoustical comparison response for rigid orifice and gates

The acoustic response given by the hydrophone signal for both rigid and gate orifices for a solitary bubble are shown in Fig. 2. The left-hand signal shows a typical freely-oscillating lightly-damped bubble acoustic emission as a bubble escapes from a rigid glass capillary tube; here the acoustic amplitude decays as $\exp[-(f_0\delta t/2)]$ as in any classical damped oscillator, in where $f_0$ is the resonant frequency and $\delta$ the damping factor. The maximum amplitude is reached in the first few milliseconds and subsequently decays (e.g. Minnaert, 1933). For the right-hand signal, a passive emission as quantitatively described previously is noted at time (*b*), but it now has different characteristics (*a*). Because this signal precedes the oscillation associated with the bubble formation, we hypothesize that this signal is related to the sediment bed characteristics of the sediment bed, and may be due to fracturing, particle mobility, etc., but to be definitive, it would be necessary to correlate this signal with the video images.

Approaches to analysis of various signals include the Fourier Transform Analysis (*FFT*) and the Spectrogram. The spectrogram or sonogram is a visual representation of the spectrum of frequencies a sound or other signals as they vary with time or some other variable. The spectrogram is calculated from the time signal using the FFT. Digitally sampled data, in the time domain, is broken up into segments in time, which usually overlap, and Fourier transformed to calculate the magnitude of the frequency spectrum for each segments. Each segment then corresponds to a vertical line in the image; a measurement of magnitude versus frequency for a specific moment in time. A time series, FFT and Spectrogram for the gate-orifice are shown in Fig. 3A–D respectively; these methodologies were applied to 3 min of recorded signal ( $\approx$ 90 bubbles), digitized at 44.1 kHz (which satisfies adequately the Nyquist criterion), implying $1.32\times10^5$ data points. The *FFT* size was 65,536 and a Hanning–Gaussian window was applied to the acoustical data using MatLab Signal Processing Toolbox R2010b (MathWorks 1984-2010, U.S.). This analysis used two audio filters; a low-pass filter (0.100–0.250 kHz) to eliminate noise attributable to the air pump and a high-pass filter (3.0–4.0 kHz) to remove external noise caused by laboratory equipment (fluorescent lamp coil, motors, etc.). A preliminary *FFT* study revealed that the acoustic signal when no bubbles are generated (noise from the floor bed) reports an important peak in a bandwidth of 0.150–0.240 kHz (Fig. 3E) which confirms that appropriate filters were selected. In a practical, seabed deployment, filtering out signals below about 1 kHz would also remove low-frequency signals corresponding to the rate of the formation of individual bubbles (Leifer and Tang, 2007). The *FFT* reveals two important peaks at about at 0.479 kHz, 2.055 kHz and small peaks around of 1.236 kHz which are in agreement with the colored elliptic zones in the spectrogram (the color indicates the sound intensity employing a linear scale). However, it can be noted that the medium-frequency sound emission is significantly shorter in duration than the high or low frequency sounds. A separate study of each pulse in the gate-orifice behavior (Fig. 4) indicates that the peaks in the *FFT* correspond to frequencies at (a) of 2.055 kHz and at (b) of 0.479 kHz. To obtain the Minnaert frequency for pulse (b) we also utilized the protocol (Manasseh et al., 2001) in which only the first period of the signal (b) was taken. This results in $f_0 \approx 0.5$ kHz. This protocol is thought to reduce errors due to the acoustic interactions of bubbles when bubbles are formed rapidly and are close together (Manasseh and Ooi, 2009).

### 3.2. Gas–granular media interaction (mechanical response by growth of a solitary bubble)

A single video-acoustic synchronized experiment in the water tank is shown in Fig. 5. When the acoustic signal is minimal no bubbles were observed (0 ms). From 5 to 10 ms, an oscillatory signal with a high frequency (a) was observed; the photographic series shows a bubble front appearing in the sediment (the first stage of the gate behavior). Subsequently, a bubble–sediment interaction occurred, in which the tezontle particles were pushed sideways by the gas and a gate-orifice was created (video image history until to 12 ms). Finally at 14 ms the bubble neck was broken, the superficial bubble area–granular media interaction finished and a typical damped passive bubble-acoustic signal in (b) was registered.

### 3.3. Photographic vs. acoustical methods (applicable to solitary bubble growth)

In order to check the Minnaert prediction equation (2), the photographic method was used to obtain the bubble size. A close-up of the bubble ($800\times600$ at 8-bit greyscale) after detachment was treated with an ImageJ image analysis routine. The bubble area was approximated by an equivalent-spherical assumption and an equivalent mean spherical radius was computed for 100 bubbles, giving $R_0=5.4$ mm with a 1–2% standard deviation. Now using $R_0$ in Eq. (2), the implied Minnaert frequency was $f'_0 \approx 0.555$ kHz. This does not have exactly the same value estimated from (b) by the first-period protocol, $f_0=0.5$ kHz, corresponding to a bubble size of 6 mm. The 10% difference between the $f_0$ and $f'_0$ frequencies may be due to a systematic error in the photographic bubble size because the bubble is not spherically symmetric. The *PA* methods are based on the bubble's volume, and are only marginally affected by distortions away from sphericity (Strasberg, 1953). The Minnaert relation only considers the volumetric change a pulsating spherical bubble, in which the bubble wall describes changes in the radium of small amplitude. Thus, systematic error in the acoustic bubble size owing to non-sphericity is less likely than systematic error in the photographic sizing owing to non-sphericity. The presence of a rigid wall is

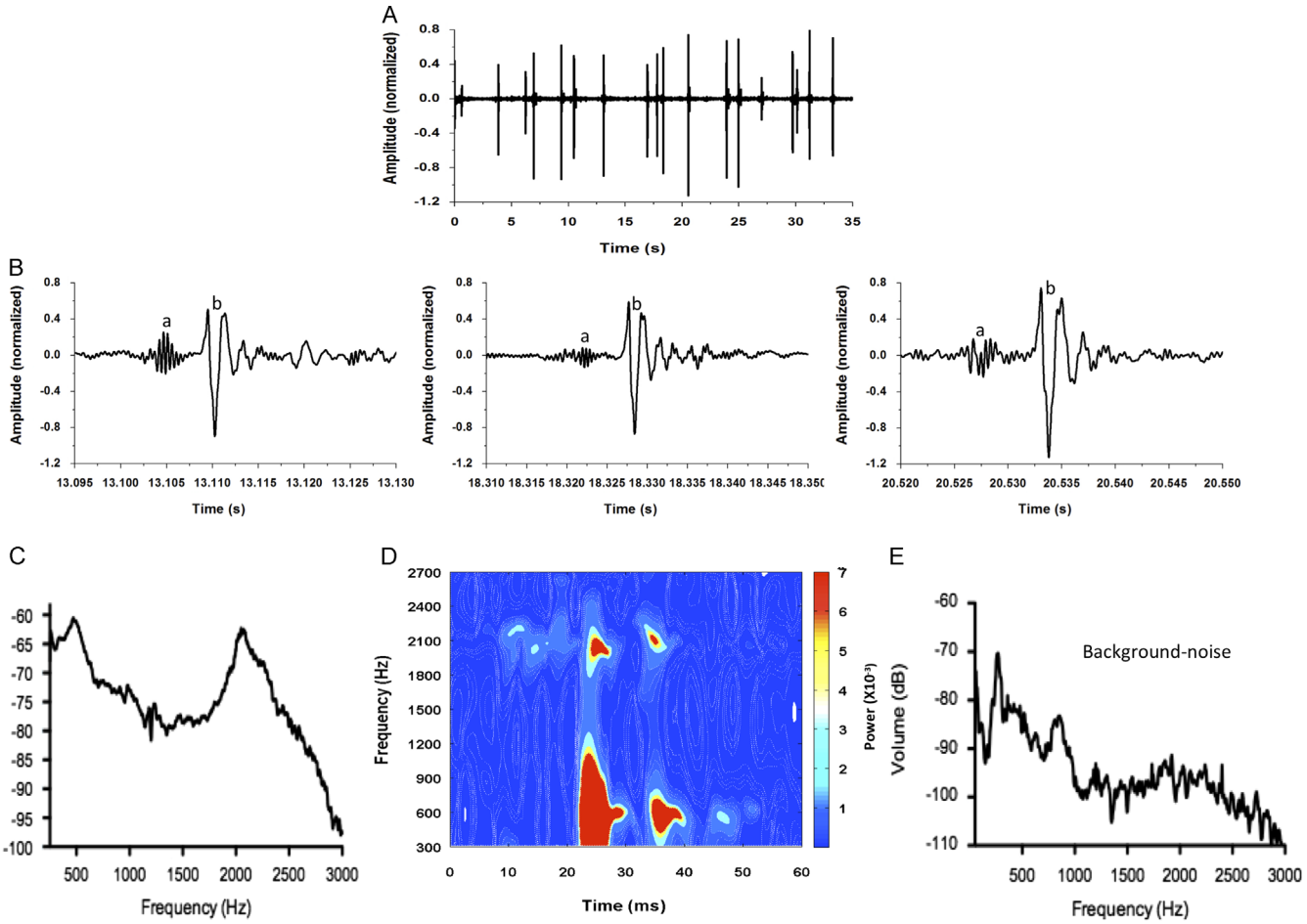


**Fig. 3.** Hydrophone recorded data (A), representative acoustic sediment-signals (B), identification of frequencies for the gate-orifice signal using *FFT* (C) and Spectragram analyses (D), and *FFT* plot by background noise (E). (For interpretation of the references to color in this figure, the reader is referred to the web version of this article.)

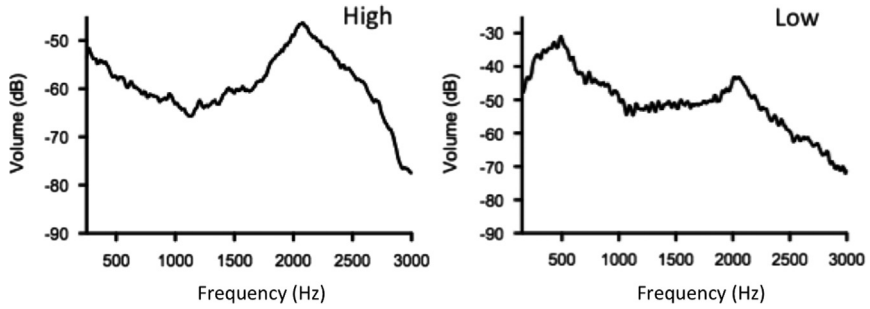


**Fig. 4.** FFT results for acoustical signal observed for sound pulses in incise (a) and (b) respectively.

known theoretically (Strasberg, 1953) and experimentally (Payne et al., 2011) to reduce the bubble frequency, so it is possible that the proximity of the granular material surfaces could also contribute to the frequency being slightly lower than expected.

### 3.4. Gas flow rates

In order to observe the acoustical response and orifice behavior when the gas flow rate is changed, low (0.5 $cm^3/s$), medium (2.5 $cm^3/s$), and high (4.5 $cm^3/s$) air flows in the sediment bed were tested. In Fig. 6 (upper diagram), the *FFT* for these three cases are indicated. For the low rate the *FFT* shows three peaks at 0.473, 1.195 and 2.056 kHz respectively; the first and last peaks have a high intensity while the second at about 1.2 kHz has a lower intensity. This is very similar to the behavior observed in Fig. 3 for a solitary bubble. For the medium air flow, the *FFT* shows that the magnitude of the highest- and lowest-frequency peaks indicated in the previous case are now interchanged, and several small intermediate peaks are observed, although a narrow spike remains at about 1.2 kHz. Finally at the high flow rate the predominant peaks return to the same form as at the low flow rate and the intermediate peaks are significantly decreased. It is interesting to observe that when the gas flow rate is increased, the predominant peaks (at the low and high extremes of the *FFT* spectrum) rise in intensity much more than intermediate peaks.

Further information was extracted by a sonogram analysis (visual representation of the acoustical signals) for each gas flow case (Fig. 6, below part). In the sonogram for the low flow-rate case, two intense light blue-red zones are observed, which represent the peaks in the *FFT*. However, it can now be seen that

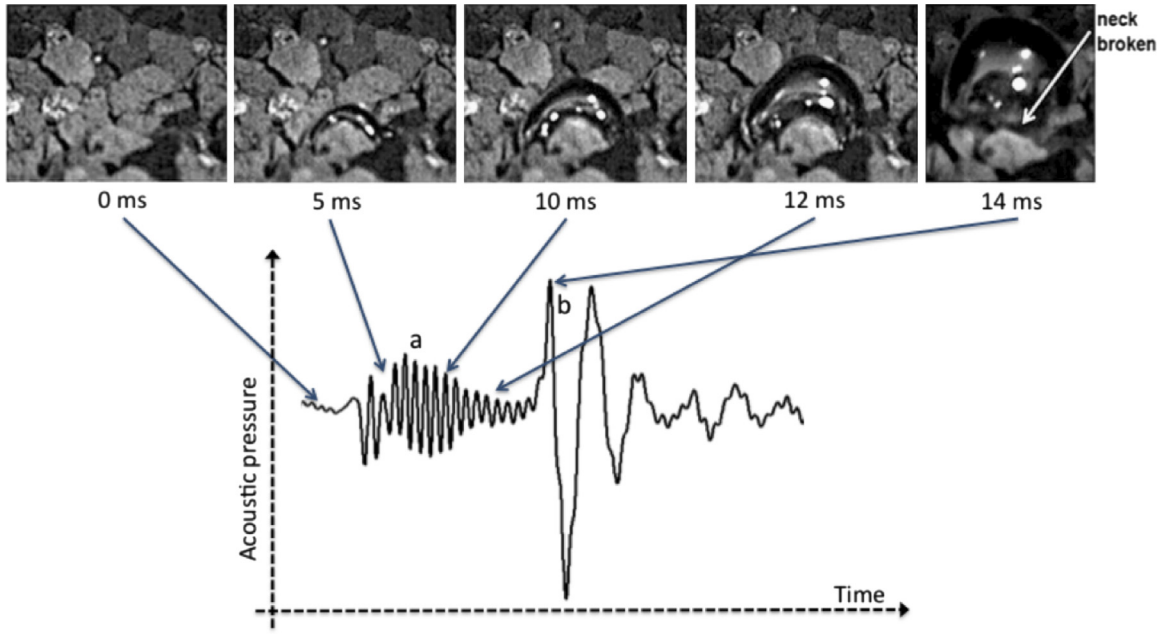


**Fig. 5.** Simultaneously acquired photos of bubble and acoustic signals for the sediment bed case.

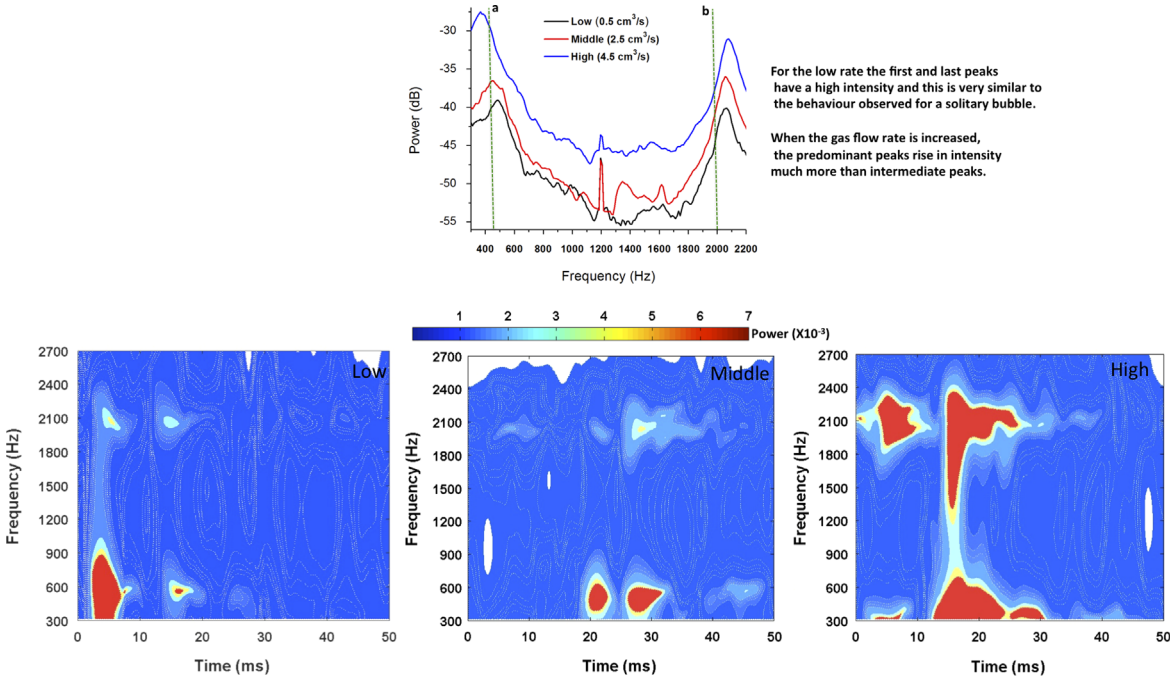


**Fig. 6.** *FFT* (above) and sonograms (below) for low, medium and high gas flow rates respectively.

the spot corresponding to the low-frequency is more disperse with respect to the high-frequency and that this sound emission occurs first, and a short time later the acoustic signal with the highest-frequency emission arrives; this temporal separation in the lowest- and highest-frequency sound signals is consistent with the 'gate' sediment behavior indicated in Fig. 5. In addition, the lowest frequency (Fig. 5(b)) has a greater acoustic pressure than the highest frequency (Fig. 5(a)), and these characteristics report the mechanical response of the sediment in the first 0–12 ms. For the medium flow-rate case, two significant light blue-red zones can be observed again in the sonogram but are now more delayed in time. By comparison with the previous, low flow-rate case, it can be inferred that they also correspond to the gate behavior shown at (a) and (b) in Fig. 5. But now, the spot assigned to the bubble detachment (low frequency) is less scattered. The sonogram in the high gas flow-rate case indicates two significant intense-disperse orange-red zones (Fig. 6, below part); again, the lowest frequency corresponds to the sound signal in (b) and the highest frequency sound emission corresponds to the signal in (a); these frequencies are correlated with the *FFT* (Fig. 6, upper part). In this case a connecting-bridge light blue-red region was observed, which corresponds to the intermediate peaks in the *FFT* in Fig. 6.

## 4. Discussion

The synchronous images and audio signal recording shown in Fig. 5 suggest that the sediment bed affects the bubble growth and

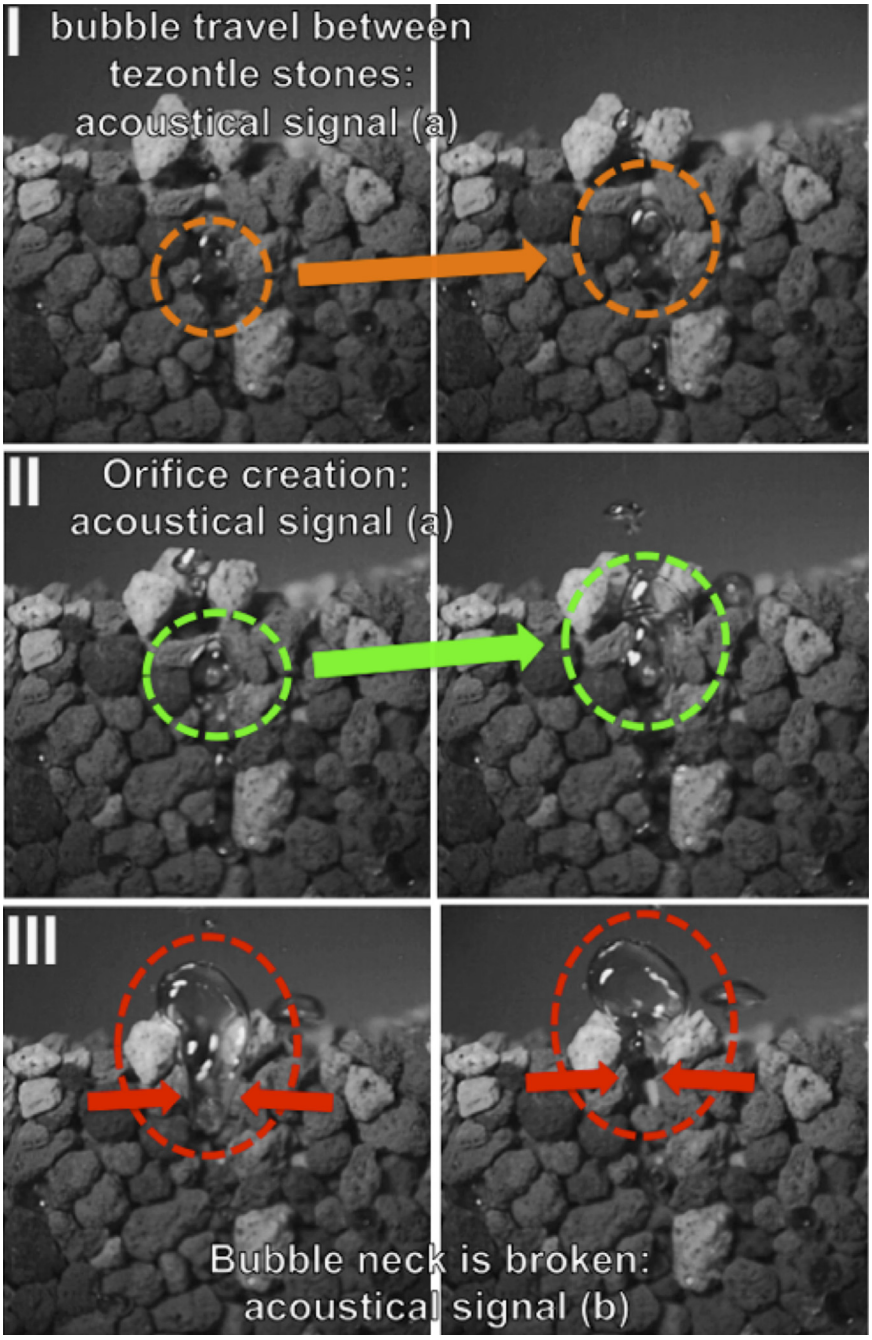


**Fig. 7.** First (I), Second (II) and Third (III) stages in the sediment behavior (profile view) correlated with sound frequencies (a) and (b) respectively.

that the various signatures in the signal can be understood as the granular media interacting with the gas. Considering first the results on the solitary bubble behavior (Fig. 2), we divided the behavior into two stages using a lateral video recording (Fig. 7). In the first stage (Fig. 7-I), an oscillatory sound signal (Fig. 2a) is registered even though no bubble is observed in the images; we propose that this sound is caused by the internal particle movement owing to gas migration through the water-filled pores. Thus the sound signal in this stage could indicate the formation of a sediment pathway or fracture of the sediment skeleton (dashed circle in Fig. 7-I) (Kong et al., 2010). For the present study all the gas injection flow rates can be considered low, insofar as the viscous force is negligible and the gas invasion is dominated by capillary forces. Under these circumstances, the capillary fingering is characterized by the observations of Lenormand et al. (1988), in which a piston-like motion develops and the gas follows the path of least resistance. It is interesting to speculate on whether this high-frequency signal ($a$, 2.055 kHz) is due to gas passing through a channel, to particle-friction movements or to vibrations of small fractions of the trapped gas volume. Future research to elucidate this stage is suggested.

The second stage (Fig. 7-II) corresponds to the pulse oscillating at $a=2.055$ kHz (Fig. 2). This coincides with the orifice creation because the tezontle stones are raised and moved horizontally (shown by the displacement of the in dashed circle); in addition the high-speed imaging in Fig. 5 shows that particles slip on the bubble surface. This can be interpreted as if the sediment presents a medium that elastically resists expansion of the bubbles and this interaction leads to bubbles that are not spherical.

The third stage (Fig. 7-III) begins when a classical Minnaert bubble emission oscillation is observed ($b=0.479$ kHz, in Fig. 2) as

the bubble neck is broken (dashed circle in Fig. 7-III). The bubble leaves the gate-orifice and the signal can be used to estimate the bubble size.

Thus, the air bubble growth through a sediment bed under quiescent water is affected by the mechanical proprieties of granular media. The acoustic signal revealed two phenomenological stages: fracture advancing-elastic resistance to orifice creation and asymmetric bubble detachment (observed by high speed video recording).

Leifer and Culling (2010) realized laboratory studies of seep bubble plumes using fixed stainless-steel capillary tubes and percolated air through diverse grain-sized sediment beds (mean radius 0.03–0.77 cm) at three air flows (6.4, 6.9 and 8.1 $cm^3/s$). Using high-speed video, they observed that the bubbles moved sediment grains and lifted them several centimeters. They also reported that during formation the bubbles were deformed dramatically leading to the pinching-off of one or two smaller bubbles, which eventually lead to the observation of coalescence. The study concluded that sediment retention ability was inversely related to sediment grain size.

The principal contributions to the acoustical signature would be the gas fracture advancing and the elastic resistance of the granular bed; the Minnaert frequency (low-frequency peak of *FFT* in Fig. 6) owing to bubble formation is also observed. Considering variations in the gas flow rate, the spectrogram results (Fig. 6) suggest that when the bubble-production rate are in the low and middle ranges (0.5–2.5 $cm^3/s$), the gate-orifice behavior is predominant because the results are very similar to those observed for the solitary-bubble case (Fig. 3). It is well known that increases in gas flow rate to a rigid underwater orifice can be manifested by various regimes in which the bubble production rate increases without significant alteration in bubble size, or the bubble size increases without significant alteration in bubble production rate, or both bubble production rate and bubble size increase (Vazquez et al., 2008). Furthermore, the experimental observations in the tezontle bed indicate that at the middle and high gas-flow rates, bubbles of large size are produced and owing to the irregularity of the surrounding media, the bubble neck is not formed reproducibly. The breaking of the bubble neck defines the resulting bubble size and hence the Minnaert frequency. This intermittency in the bubble neck formation can be represented by the formation of new peaks in the intermediate region (1.3–1.7 Hz) in the *FFT* in Fig. 6; it can be inferred that the bubble size in the middle regime is no longer monodispersed. In the high gas-flow case, more bubbles are growing in the sediment, they are larger and it is possible that they could coalesce and this may explain by the observation of the bridge between the main regions observed in the spectrogram from Fig. 6. It is possible that at the high flow rate, alterations in the bed elasticity (more gas passing through the sediment) could be manifested by alterations in the highest frequency peaks, this may explain the large dispersion for the frequency range of 1.8–2.4 kHz observed in the spectrogram in Fig. 6. Finally, this behavior suggests that a gas jet has formed at the orifice-rim, rather than the discrete bubble formation from the orifice that occurs at lower gas-flow rates. Therefore, the gas jet prevents the stones in the surface from falling back to close the orifice (gate). This can be interpreted as if the sediment bed becomes a temporary rigid orifice network, but it is unstable because in the particles in the surface change location over a short time scale.

For the solitary bubble case, the data suggest that the Minnaert relation is a reasonable choice to obtain the bubble size generated in this type of medium, provided the signal is appropriately windowed to the bubble-detachment event, to separate the signal yielding the bubble size from sounds due to the sediment particle motion. For accurate quantitative data, careful time-domain windowing of the acoustic pulses in a manner similar to earlier studies (Al-Masry et al., 2005) would be necessary. Of course, this should be followed by appropriate statistical averaging to generate statistical confidence limits on $R_0$ and $f_b$. While these could vary from site to site, an initial, in situ calibration would appear feasible, in which a submersible places a hydrophone near a particular seep and local imaging estimates the initial bubble size.

In most practical cases of relevance to global warming or earthquake prediction, it is the change relative to an initial baseline that is of relevance. As long as the initial baseline is reliably determined to be dominated by the bubble signal, rather than that of the surrounding sediment, changes may be determined. Of course, the baseline signal may suffer from a high intrinsic variability. However, when statistical data on bubble sound-emission frequencies are collected over sufficiently long periods of time such that a sufficiently large number of individual frequency measurements are made, variations in the mean or in other statistical moments that represent a real change in the physics can be detected with 95% statistical confidence. This has been demonstrated in industrial bubbling systems in which changes occur over a 24-h period (Manasseh and Ooi, 2009). If physically-meaningful changes over months or years is of interest, passive acoustics has the potential to collect enough data to warn that some physical change in the system has occurred. Unlike active devices (such as sonar-arrays, multibeam-echo sounding, etc.), hydrophones that passively 'listen' are inexpensive and could be easily installed in underwater arrays. It is important to clarify that the passive technique may be considered "inexpensive" or "easy" compared to other techniques used for monitoring a marine methane seep, but it is well known to oceanographers that an array of hydrophones involves non-trivial requirements which can imply a significant budget (cable to shore, cable to a surface buoy or underwater acoustic communications link to a surface-expressed receiver, ships for deployment, installation and maintenance of the hydrophone, etc.).

Once gas flow rates increase to significantly higher levels, the sediment-bed signals appear to dominate the bubble-acoustic signals. This emphasizes the importance of distinguishing between the bubble acoustics and the sediment acoustics in an initial in situ calibration.

## 5. Conclusions

The present study has identified the acoustical signature when an air bubble is formed in a granular-sediment bed. We found that the air bubble growth through a sediment bed under quiescent water is affected by the mechanical proprieties of granular media. Moreover, the acoustic signal revealed two phenomenological stages: fracture advancing-elastic resistance to orifice creation and asymmetric bubble detachment.

Careful observations using both spectral and spectrogram approaches as well as examinations of the time-series indicate that the duration of the signal as well as its frequencies are affected by the presence of the sediment bed.

In addition, when bubbles are produced from an underwater orifice at low to middle rates, they are formed as a series of discrete pulses. This means that two classes of data are available, the bubble size estimated from each pulse, and the rate of bubble production obtained by simply counting the pulses. Together, these two sources of data would easily be recorded by robust, sea-bed hydrophones, which could be deployed in unstable environments to monitor the release of methane or other gases over long time periods.

Pulses of sound attributable to the presence of the sediment interacting with the gas contribute significant power to the overall

signal. Nonetheless, for low to medium gas-flow rates, the signal displaying the Minnaert frequency of the newly-formed bubble can be extracted by appropriate windowing in the time domain, and, where appropriate, filtering in the frequency domain. High gas-flow rates may produce signals dominated by sediment motion. It is possible that the present experiment, with millimetre-sized stones, may represent a worst case for sizing bubbles in a sediment bed that may have much finer-grained sediment.

Only one type of sediment bed was investigated in the present study. There should be a systematic survey of different particle sizes and characteristics.

In a practical deployment, appropriate siting of hydrophones near to active, low to medium flow rate seeps may result in the most sensitive indicator of change. An initial in situ calibration would enable appropriate filter settings that only pass the bubble-acoustic signals relevant to bubble sizing. Over hours or days, accurate statistics on bubble sizes and bubble formation rates would be collected. In summary, the answer to the question posed by this paper's title is affirmative, provided the hydrophone system is appropriately placed and calibrated in situ.

## Nomenclature

| | |
|---|---|
| $A$ | image area, $mm^2$ |
| $f_{bi}$ | bubble rate, bubbles $s^{-1}$ |
| $f_0$ | resonant frequency, Hz |
| $N$ | number of bubbles, bubbles |
| $P_A$ | liquid pressure, Pa |
| $Q$ | volumetric gas flow, $cm^3\ s^{-1}$ |
| $R_0$ | equivalent-spherical bubble radius, mm |
| $t$ | time, s |
| $\gamma$ | specific heats ratio, dimensionless |
| $\delta$ | damping factor |
| $\rho$ | liquid density, $kg/m^3$ |

## Acknowledgments

The authors gratefully acknowledge Prof. Ira Leifer for the technical assistance in the MatLab routines by the sound signal analysis.

## References

Al-Masry, W., Ali, E., Aqeel, Y., 2005. Determination of bubble characteristics in bubble columns using statistical analysis of acoustics sound measurements. Chem. Eng. Res. Des. 83, 1196–1207.

Arndt, J.E., Schenke, H.W., Jakobsson, M., Nitsche, F.O., Buys, G., Goleby, B., Rebesco, M., Bohoyo, F., Hong, J., Black, J., Greku, R., Udintsev, G., Barrios, F., Reynoso-Peralta, W., Taisei, M., Wigley, R., 2013. The International Bathymetric chart of the southern ocean (IBCSO) version 1.0—a new bathymetric compilation covering circum-antarctic waters. Geophys. Res. Lett. 40 (12), 3111–3117.

Artemov, Y.G., Egorov, V.N., Polikarpov, G.G., Gulin, S.B., 2007. Methane emission to the hydro - and atmosphere by gas bubble streams in the Dnieper paleo-delta, the Black Sea. Rep. Natl. Acad. Sci. Ukr. 5, 110–116 (in Russian).

Boudreau, B.P., Algar, C., Johnson, B.D., Croudace, I., Reed, A., Furukawa, Y., Dorgan, K.M., Jumars, P.A., Grader, A.S., 2005. Bubble growth and rise in soft sediments. Geological Society of America 33, 517–520.

Boyd, W.R.J., Varley, J., 2001. The uses of passive measurement of acoustic emissions from chemical engineering processes. Chem. Eng. Sci. 56 (5), 1749–1767.

Chicharro, R., Vazquez, A., 2014. The acoustic signature of gas bubbles in a liquid cross-flow. Exp. Therm. Fluid Sci 55, 221–227.

Czerski, H., Deane, G.B., 2011. The effect of coupling on bubble fragmentation acoustics. J. Acoust. Soc. Am. 129 (1), 74–84. http://dx.doi.org/10.1121/1.3514416.

Deane, G.B., Czerski, H., 2008. A mechanism stimulating sound production from air bubbles released from a nozzle. J. Acoust. Soc. Am. 123 (6), El126–El132. http://dx.doi.org/10.1121/1.2908198.

Deane, G. B., & Stokes, M. D. (2008). The acoustic excitation of air bubbles fragmenting in sheared flow. J. Acoust. Soc. Am., 124(6), 3450–3463. 10.1121/1.3003076.

Floodgate, G.D., Judd, A.G., 1992. The origins of shallow gas. Cont. Shelf Res. 12, 1145–1156.

Fu, C.C., Yang, T.F., Walia, V., Chen, C.H., 2005. Reconnaissance of soil gas composition over the buried fault and fracture zone in southern Taiwan. Geochem. J. 39 (5), 427–439.

Gostiaux, L., Gayvallet, H., Gérminard, J-C., 2002. Dynamics of a gas rising through a thin immersed layer of granular material: an experimental study. Granul. Matter 4, 39–44.

Hartmann, J., Levy, J.K., 2005. Hydrogeological and gasgeochemical earthquake precursors – a review for application. Nat. Hazards 34 (3), 279–304.

Judd, A.G., 2004. Natural seabed gas seeps as sources of atmospheric methane. Environ. Geol. 30 (46), 988–996.

Judd, A.G., Hovland, M., 2007. Seabed Fluid Flow. Cambridge University Press, Cambridgehttp://dx.doi.org/10.1017/CBO9780511535918.

Khilyuk, L.F., Chilingar, G.V., 2000. Gas Migration: Events Preceding Earthquakes. Gulf Professional Publishing 088415300.

Klusman, R.W., Webster, J.D., 1981. Meteorological noise in crustal gas emission and relevance to geochemical exploration. J Geochem. Explor. 15, 63–76.

Kolaini, R.A.,., 1999. Effects of salt on bubble acoustic radiation in water. J. Acoust. Soc. Am. 105 (4), 2181–2186.

Kong, X-Z., Kinzelbach, W., Stauffer, F., 2010. Morphodynamics during air injection into water-saturated movable spherical granulates. Chem. Eng. Sci. 65, 4652–4660.

Lange, N.A., 1999. Langes Handbook of chemistry. McGraw-Hill, New York.

Leifer, I., Culling, D., 2010. Formation of seep bubble plumes in the Coal Oil Point seep field. GeoMarine Lett. 30 (3-4), 339–353.

Leifer, I., Tang, D., 2007. The acoustic signature of marine seep bubbles. J. Acoust. Soc. Am. 121 (1), 35–40.

Leighton, TG., 1994. The acoustic bubble, p. xxvi, 613 pp.). Academic Press, London.

Leighton, T.G., Fagan, K.J., Field, J.E., 1991. Acoustic and photographic studies of injected bubbles. Eur. J. Phys. 12 (2), 77–85.

Leighton, T.G., White, P.R., 2012. Quantification of undersea gas leaks from carbon capture and storage facilities, from pipelines and from methane seeps, by their acoustics emissions. Proc. R. Soc. A 468, 485–510. http://dx.doi.org/10.1098/rspa.2011.0221.

Lenormand, R., Touboul, E., Zarcone, C., 1988. Numerical models and experiments on immiscible displacement in porous media. Fluid Mech. 189, 165–187.

MacGuire, A.D., Chapin-III, F.S., Walsh, J.E., Wirth, C., 2006. Integrated regional changes in arctic climate feedbacks: Implications for the global climate system. Annu. Rev. Environ. Resour. 31 (1), 61–91.

Manasseh, R., La Fontaine, R.F., Davy, J., Sheperd, I., Zhu, Y.G., 2001. Passive acoustic bubble sizing in sparged systems. Experiments in Fluids 30, 672–682.

Manasseh, R., Riboux, G, Risso, F., 2008. Sound generation on bubble coalescence following detachment. Int. J. Multiph. Flows 34, 938949.

Manasseh, R., Ooi, A, 2009. Frequencies of acoustically interacting bubbles. 1. Bubble Sci. Eng. Technol., pp. 58–74.

Matveeva, T., Soloviev, V.A., Wallmann, K., Obzhirov, A., Biebow, N., Poort, J., Salomatin, A., Shoji, H., 2003. Geochemistry of gas hydrate accumulation offshore NE Sakhalin Island (the Sea of Okhotsk): results from the KOMEX-2002 cruise. Geo Mar. Lett. 23, 278–288. http://dx.doi.org/10.1007/s00367-003-0150-1.

Minnaert, M., 1933. On musical air-bubbles and sounds of running water. Philos. Mag. 16, 235–248.

Nikolovska, A., Shaling, H., Bohrmann, G., 2008. Hydroacoustic methodology for detection, localization, and quantification of gas bubbles rising from the seafloor at gas seeps from the eastern Black Sea. Geochem. Geophys. Geosyst. 9 (Q10010).

Nikolovska A., Waldmann C. 2006 Passive acoustic quantification of underwater gas seepage OCEANS, Boston, 18–21 September 2006 6 New York, NY Institute of Electrical and Electronic Engineers http://dx.doi.org/10.1109/OCEANS.2006.306926.

Papastefanou, C., 2007. Measuring radon in soil gas and groundwaters: a review. Ann. Geophys. 50 (4), 569–578.

Payne, E., Ooi, A., Manasseh, R, 2011. Insonation frequency selection may assist detection and therapeutic delivery of targeted ultrasound contrast agents. Ther. Deliv. 2 (2), 213–222.

Schneider von Deimling, J., Brockhoff, J., Greinert, J., 2007. Flare imaging with multiple systems: data processing for bubble detection at seeps. Geochem. Geophys. Geosyst. 8, Q06004. http://dx.doi.org/10.1029/2007GC001577.

Shakhova, N., Semiletov, I., Panteleev, G., 2005. The distribution of methane on the Siberian Arctic shelves: implications for the marine methane cycle. Geophys. Res. Lett. 32, 9.

Sugisaki, R., 1981. Deep-seated gas emission induced by the earth tide – a basic observation for geochemical earthquake prediction. Science 212 (4500), 1264–1266.

Strasberg, M., 1953. The pulsation frequency of nonspherical gas bubbles in liquid. J. Acoust. Soc. Am. 25 (3), 536–537.

Vazquez, A., Leifer, I., Sanchez, R.M., 2010. Consideration of the dynamic forces during bubble growth in a capillary tube. Chem. Eng. Sci. 65 (13), 4046–4054.
Vazquez, A., Manasseh, R., Sánchez, R.M., Metcalfe, G., 2008. Experimental comparison between acoustic and pressure signals from a bubbling flow. Chem. Eng. Sci. 63, 5860–5869.
Vazquez, A., Sanchez, R.M., Salinas-Rodríguez, E., Soria, A., Manaseeh, R., 2005. A look at three measurement techniques for bubbles size determination. Exp. Therm. Fluid Sci. 30, 49–57.
Webb, S.C., Deaton, T.K., Lemiere, J.C., 2001. A broadband ocean-bottom seismometer system based on a 1-Hz natural period geophone. Bull. Seismol. Soc. Am. 91 (2), 304–312.
Wilkens, R.H., Richardson, M.D., 1998. The influence of gas bubbles on sediment acoustic properties: in situ, laboratory, and theoretical results from Eckernforde Bay, baltic sea. Cont. Shelf Res. 18, 1859–1892.